

## Article

# Influence of Surface Roughness on Nanocrystalline Diamond Films Deposited by Distributed Antenna Array Microwave System on TA6V Substrates

Azadeh Valinattaj Omran <sup>1</sup>, Chaimaa Mahi <sup>1</sup>, Romain Vayron <sup>2</sup>, Céline Falentin-Daudré <sup>3</sup> and Fabien Bénédic <sup>1,\*</sup>

- <sup>1</sup> Laboratoire des Sciences des Procédés et des Matériaux, Centre National de la Recherche Scientifique (UPR 3407), Université Sorbonne Paris Nord, 93430 Villetaneuse, France; azadeh.valinattajomran@lspm.cnrs.fr (A.V.O.); chaimaa.mahi@lspm.cnrs.fr (C.M.)
- <sup>2</sup> Laboratoire d'Automatique de Mécanique et d'Informatique Industrielles et Humaines (UMR 8201), Centre National de la Recherche Scientifique, University Polytechnique Hauts-de-France, 59313 Valenciennes, France; romain.vayron@uphf.fr
- <sup>3</sup> Laboratoire de Biomatériaux Pour la Santé, Chimie, Structures, Propriétés de Biomatériaux et d'Agents Thérapeutiques, Centre National de la Recherche Scientifique (UMR 7244), Université Sorbonne Paris Nord, 93430 Villetaneuse, France; falentin-daudre@univ-paris13.fr
- \* Correspondence: fabien.benedic@lspm.cnrs.fr

**Abstract:** In this study, the characteristics of nanocrystalline diamond films synthesized at low surface temperature on Ti-6Al-4V (TA6V) substrates using a distributed antenna array microwave reactor aiming at biomedical applications were investigated. The surface roughness of the TA6V substrates is varied by scratching with emery paper of 1200, 2400, 4000 polishing grit. Nanocrystalline diamond (NCD) coatings with morphology, purity, and microstructure comparable to those obtained on silicon substrates usually employed in the same reactor and growth conditions are successfully achieved whatever the polishing protocol. However, the latter has a significant effect on the roughness parameters and hardness of the NCD films. The use of the finest polishing grit thus permits us to enhance the hardness value, which can be related to the work-hardening phenomenon arising from the polishing process.

**Keywords:** diamond; thin films; chemical vapor deposition; titanium alloys; biocompatibility



**Citation:** Valinattaj Omran, A.; Mahi, C.; Vayron, R.; Falentin-Daudré, C.; Bénédic, F. Influence of Surface Roughness on Nanocrystalline Diamond Films Deposited by Distributed Antenna Array Microwave System on TA6V Substrates. *Coatings* **2023**, *13*, 1300. <https://doi.org/10.3390/coatings13071300>

Academic Editors: Ioana Demetrescu and Anca Mazare

Received: 26 June 2023  
Revised: 18 July 2023  
Accepted: 22 July 2023  
Published: 24 July 2023



**Copyright:** © 2023 by the authors. Licensee MDPI, Basel, Switzerland. This article is an open access article distributed under the terms and conditions of the Creative Commons Attribution (CC BY) license (<https://creativecommons.org/licenses/by/4.0/>).

## 1. Introduction

Biomaterials are materials intended to interface with biological systems to evaluate, treat, augment, or replace any tissue or organ of the body [1]. Among the metals used in biomaterial research, titanium (Ti) and alloys based on it are very interesting materials, owing to their excellent biocompatibility properties as well as other several outstanding properties, such as high hardness, high thermal conductivity, and good fatigue properties. However, the practical use of titanium biomaterials, such as those used as orthopedic implants, is limited because some titanium implants integrate incorrectly into the surrounding bone tissue, loosen over time, or cause severe inflammatory responses, which often requires corrective surgery. To address this problem, titanium surfaces can be modified or coated to enhance cellular behavior on the biomaterial [2–5]. Recently, nanocrystalline diamond (NCD) films have been considered as coating materials for medical devices because they combine surface smoothness, high hardness, low friction coefficient, and biocompatibility suitable for biomedical applications [6]. In our previous paper, NCD films were successfully grown at low substrate temperature on titanium flat discs using a distributed antenna array (DAA) reactor and the biocompatibility of NCD/Ti samples was studied through osteoblast cell viability and cell morphology [7]. The nanocrystalline diamond coating exhibits no sign of cytotoxicity and improves cell adhesion and spreading. It is then of prime interest to

understand which characteristics of the NCD layer (microstructure, topography, hardness, phase purity) control its biological properties.

Surface topography is an important factor which can control surface properties of carbon coatings. For example, prior measurements of diamond-like carbon (DLC) coatings show that tribological behavior [8] and adhesion [9] are strongly affected by the surface texture, all the way down to the nanoscale. In addition, the surface topography of diamond coatings [10] affects their performance, including their friction [11], wear [12], adhesion [13,14], and biocompatibility [15].

In this study, the synthesis of NCD films at low surface temperature using a DAA microwave reactor was investigated on TA6V (i.e., Ti-6Al-4V alloy), which is widely used for the fabrication of biocompatible implants. It is expected that if NCD films can be directly synthesized on the TA6V surface and good adhesion can be achieved, surface improvement in terms of high hardness, corrosion resistance, and ultimately in terms of the compatibility of metal materials with the human body can be realized. In order to examine the influence of the TA6V surface topography on the NCD film properties, the surface roughness of the TA6V substrate was varied by scratching with emery papers of different grain size. Various characterization techniques were then used in order to assess the microstructure, the roughness, and the hardness of the coatings.

## 2. Experimental Methods

### 2.1. NCD Film Synthesis

NCD films were grown on TA6V disks using a DAA reactor, the details of which can be found elsewhere [16–18]. Typical process conditions were employed to grow NCD films: a gas mixture composed of 96.4% H<sub>2</sub>, 2.6% CH<sub>4</sub>, and 1% CO<sub>2</sub> with 50 SCCM (standard cubic centimeters per minute) total flow rate at a process pressure of 0.35 mbar and a microwave power of 3 kW distributed on 16 elementary sources [19]. No heating or cooling of the substrate holder was imposed so that the substrate temperature was imposed by the plasma conditions at 270 °C. The deposition time was 5 h for all the samples, which means that, in the considered conditions, the film thickness is approximately 220 nm.

TA6V disks provided by Goodfellow Cambridge Ltd. (Huntingdon, England) were used as the substrate for NCD growth. The TA6V samples possess alpha + beta microstructure. In order to remove the layer which has been damaged by machining at the surface of the metal, mechanical polishing of TA6V surfaces was carried out using a mechanical arm mounted on a rotary polisher (LaboPol 5 polishing system from Struers, Champigny sur Marne, France). The disk surface of 1.5 cm diameter was polished with SiC emery papers provided by Fuga. Three abrasive grain sizes of 15 µm, 9 µm, and 5 µm, referenced as granulometry 1200, 2400, and 4000 in the following, respectively, were employed in order to obtain different surface topography. A first, polishing was carried out with a 500-grit SiC paper (30 µm grit) for 40 s. The polishing was then refined using a lower-grit paper of grade 1200 (15 µm grit) for 40 s. Then, to obtain granulometry 2400, the polishing was then refined using a lower-grit paper of grade 2400 (9 µm grit) for 40 s, and finally, to obtain granulometry 4000, the polishing was then refined using a lower-grit paper of grade 4000 (5 µm grit) for 40 s.

After polishing, the surfaces were cleaned in acetone overnight under stirring. The following day, the surfaces were successively cleaned once in an acetone bath and three times in a distilled water (dH<sub>2</sub>O) bath with sonication for 15 min. Then, the disks were put in Kroll's reagent (2% HF, Sigma; 10% HNO<sub>3</sub>, Acros and 88% dH<sub>2</sub>O) for one minute with stirring followed by five consecutive dH<sub>2</sub>O baths with sonication for 15 min each time. In order to promote the diamond nucleation on the TA6V surface, the substrates were finally seeded by spin coating using nanodiamond (submicron diamond) powder of 25 nm grain size powder with highly negative zeta potential (SYP-GAF-0-0.05 provided by Van Moppes, Geneva, Switzerland). The colloidal solution was diluted in water and, in order to avoid coagulation, polyvinyl alcohol (PVA) powder was added. It should be mentioned that the spin coating protocol has been optimized in order to provide reproducible, homo-

geneous, and high ( $\geq 10^{10} \text{ cm}^{-2}$ )-nucleation density, leading to the formation of continuous NCD films from a deposited thickness of 30–40 nm. Thus, the seeding procedure does not significantly affect the characteristics of NCD films with thickness higher than 200 nm.

## 2.2. Surface Analysis Techniques

The morphology of NCD film was studied by Scanning Electron Microscopy (SEM). SEM images were taken using a SUPRA 40VP (Carl Zeiss Meditec AG, Jena, Germany) system operating at 3 kV without any additional conductive coating on the NCD film.

Raman spectra were obtained with an HR800 (HORIBA Jobin Yvon IBH Ltd., Palaiseau, France) apparatus with a notch filter operating at 473 nm excitation wavelength and using a grating of 2400 grooves per mm, with spectral collection time of 2 s at an average of 2 times by a  $100\times$  microscope objective. These spectra were afterwards used to analyze the phase purity of the deposited diamond films.

XRD patterns were obtained using an ARL EQUINOXE 1000 X-ray diffractometer, from Thermo Fisher Scientific (Waltham, MA, USA). The X-ray beam used is produced by a copper anticathode at a wavelength of  $\lambda_{\text{CuK}\alpha 1} = 1.54056 \text{ \AA}$  with an incident X-ray angle of  $1^\circ$ . The film grain size was estimated using a modified Scherrer equation and Rietveld method applied on the (111) and (220) diffraction peaks [20,21].

An atomic force microscope (Dimension Icon, Bruker Corporation, Billerica, MA, USA) operating in the tapping mode was used to examine the topography and roughness of the films. A profilometer (Dektak XT-S, Bruker Corporation, Billerica, MA, USA) was employed to further investigate mechanically the coating topography with a scan length of 1000  $\mu\text{m}$ .

A white light interferometer (NewView 7300, Zygo Corporation, Middlefield, CT, USA) was employed for characterizing and quantifying the surface roughness. Optical resolutions of  $50\times$  Mirau objective were 0.52  $\mu\text{m}$  for x and y axes based on Sparrow criteria. Indeed, spatial sampling based on camera pixel size (0.55  $\mu\text{m}$ ) was lower than the optical resolution. The inspected surface area was 252  $\mu\text{m}$  by 252  $\mu\text{m}$ , obtained by stitching of each single measurement with 20% overlap. Three samples were considered for each configuration, i.e., coated and uncoated TA6V substrates polished with 3 different abrasive papers (i.e.,  $3 \times 6 = 18$  samples), and ten measurements were performed on each sample (i.e., 180 measured surfaces). The Gaussian filter has been recommended by ISO 11562-96 and ASME B46.1-95 standards for determining the mean line in surface metrology. This filter was adapted in order to filter the 3D surfaces with a given cut-off value (50  $\mu\text{m}$ ) [22]. Then 3D roughness parameters were computed and defined by the following standards: ISO 25178 defines 30 parameters, and EUR 15178N also defines 30 parameters, but some are identical to those of ISO 25178.

The surface of each specimen was evaluated by means of Vickers hardness (HV) with a microdurometer FM (Future-Tech Corp., Milan, Italy), with a load of 300 g/10 s. For each surface, five indentations were made to obtain the hardness average and standard deviation for each sample. The microhardness data were submitted to statistical analysis using a one-way ANOVA and Tukey Kramer's test ( $p < 0.05$ ) using the software of MathWorks Matlab R2019b.

## 3. Results and Discussion

The surface morphology of the NCD film-coated TA6V substrates at different polishing grades is shown in Figure 1. The whole surface is homogeneously covered by a continuous film formed of non-faceted nanometric grains and aggregates, characteristic of NCD layers obtained with a DAA microwave system and resulting from a predominant high-rate secondary nucleation growth mode [23]. One can also observe that there is no significant effect of polishing on the morphology of NCD films.

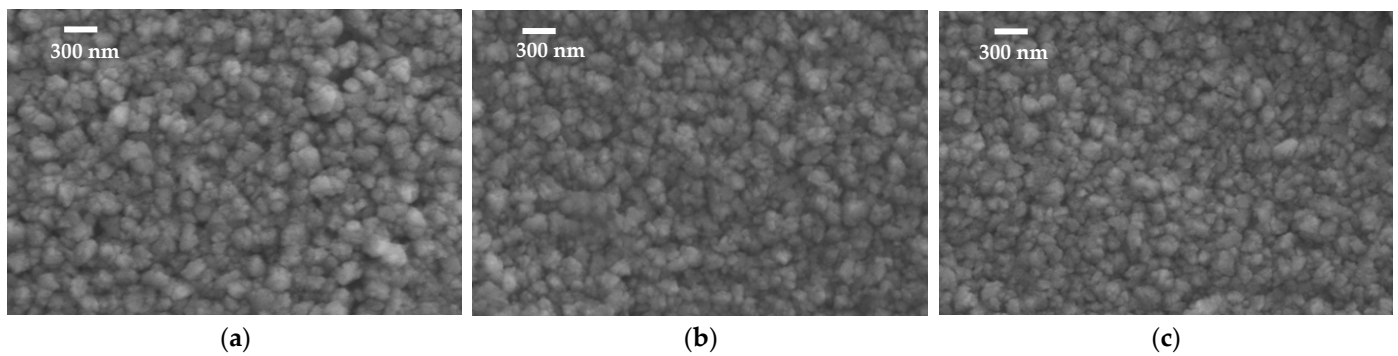


**Figure 1.** Typical SEM micrographs of diamond films grown on TA6V substrates polished with various granulometry: (a) 1200, (b) 2400, and (c) 4000.

These observations are confirmed by the AFM observations of the surface morphological behavior after the different polishings and coatings (Figure 2).

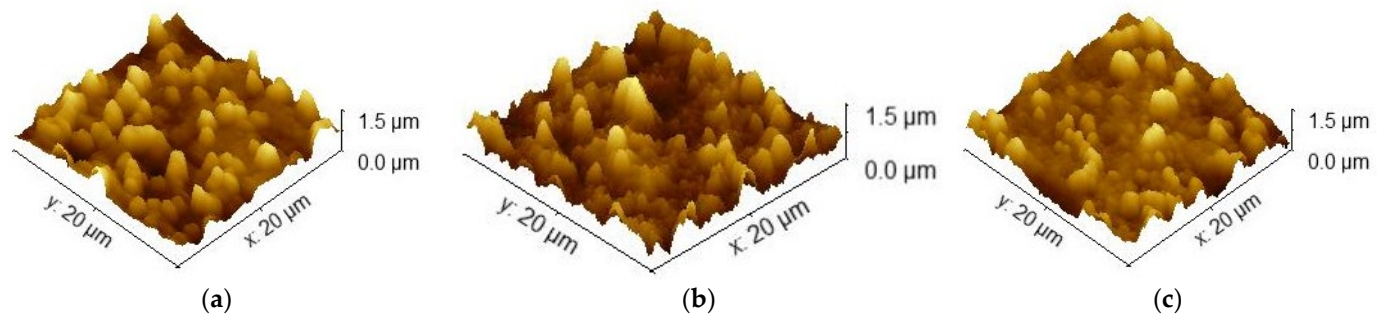


**Figure 2.** AFM micrographs of diamond films grown on TA6V substrates polished with various granulometry: (a) 1200, (b) 2400, and (c) 4000.

Raman spectroscopy permits us to confirm the growth of diamond layers on the TA6V substrates, as shown in Figure 3. All spectra exhibit a diamond characteristic peak at  $1332\text{ cm}^{-1}$ , which is further evidence for the diamond nature of the films. The Full Width at Half Maximum (FWHM) of the diamond peaks for different polishing conditions is above  $10\text{ cm}^{-1}$ , which is characteristic of the nanocrystalline feature. The spectra also show broad bands around  $1350$  and  $1580\text{ cm}^{-1}$ , attributed to graphite D band (breathing mode of  $\text{sp}^2$ -carbon rings arising in the presence of defects in graphite edges) and graphite G band (E 2g vibrational mode arising from  $\text{C}(\text{sp}^2)\text{--C}(\text{sp}^2)$  bonds), respectively [24]. The contributions of the Trans-polyacetylene (TPA) responses around  $1140\text{ cm}^{-1}$  (C-H in plane bending) and  $1480\text{ cm}^{-1}$  (C=C stretch) [25] are not so obvious.

For all the polishing conditions, the diamond content  $\text{sp}^3$  (%) was calculated using the ratio of the diamond peak to the diamond and non-diamond contributions following the procedure reported in [26]. As described in this paper, in addition to the diamond peak, seven major non-diamond bands were considered. Several identified small non-diamond peaks were also integrated into the sum of non-diamond contributions, such as the one at  $1570\text{ cm}^{-1}$  visible on the spectrum acquired for granulometry 4000. The  $\text{sp}^3$  (%) was then estimated at  $91\% \pm 5\%$ ,  $89\% \pm 4\%$ , and  $83\% \pm 4\%$  for polishing granulometry of 1200, 2400, and 4000, respectively. This is satisfactory in terms of purity and comparable to the values obtained for NCD films deposited at low temperature on silicon substrates, which are typically greater than or equal to 70% for a deposition temperature of  $400\text{ }^\circ\text{C}$  [23]. Considering the standard deviation, the diamond content estimated here is roughly constant, which demonstrates that there is no significant influence of the polishing grain size on the NCD film purity.

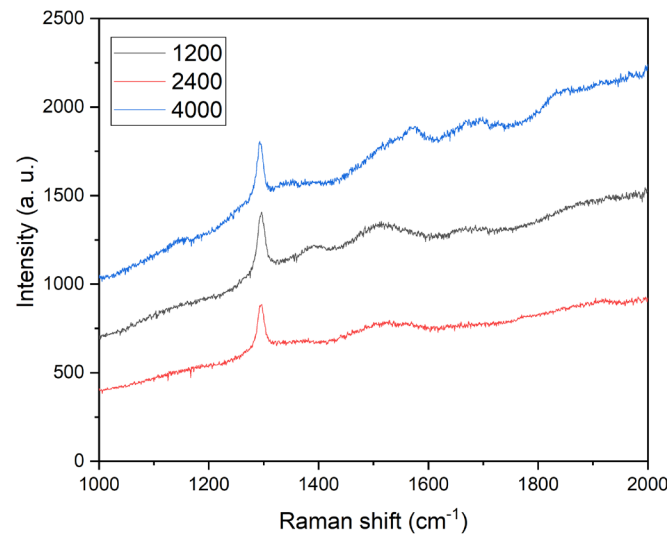


**Figure 3.** Typical Raman spectra of diamond thin films grown on TA6V substrates polished with the three investigated granulometries.

X-ray diffraction patterns of the NCD coatings for the three polishing grain sizes are shown in Figure 4a. All the coatings exhibit the (1 1 1), (2 2 0), and (3 1 1) diffraction peaks of diamond occurring at  $2\theta = 43.9^\circ$ ,  $2\theta = 75.3^\circ$ , and  $2\theta = 91.5^\circ$ , respectively (JCPDS card 79-1467). This confirms the presence of crystalline diamond within the films. The other peaks occurring at  $2\theta = 34.5^\circ$ ,  $2\theta = 39.5^\circ$ , and  $2\theta = 62^\circ$  are related to titanium in alpha phase [27]. In order to probe the diamond grain size for all the operating conditions considered here, the size of coherent diffracting domains was estimated from XRD patterns through the Rietveld method. Figure 4b shows that the grain size remains approximately constant for the different polishing grain sizes, with values between 10 and 15 nm.

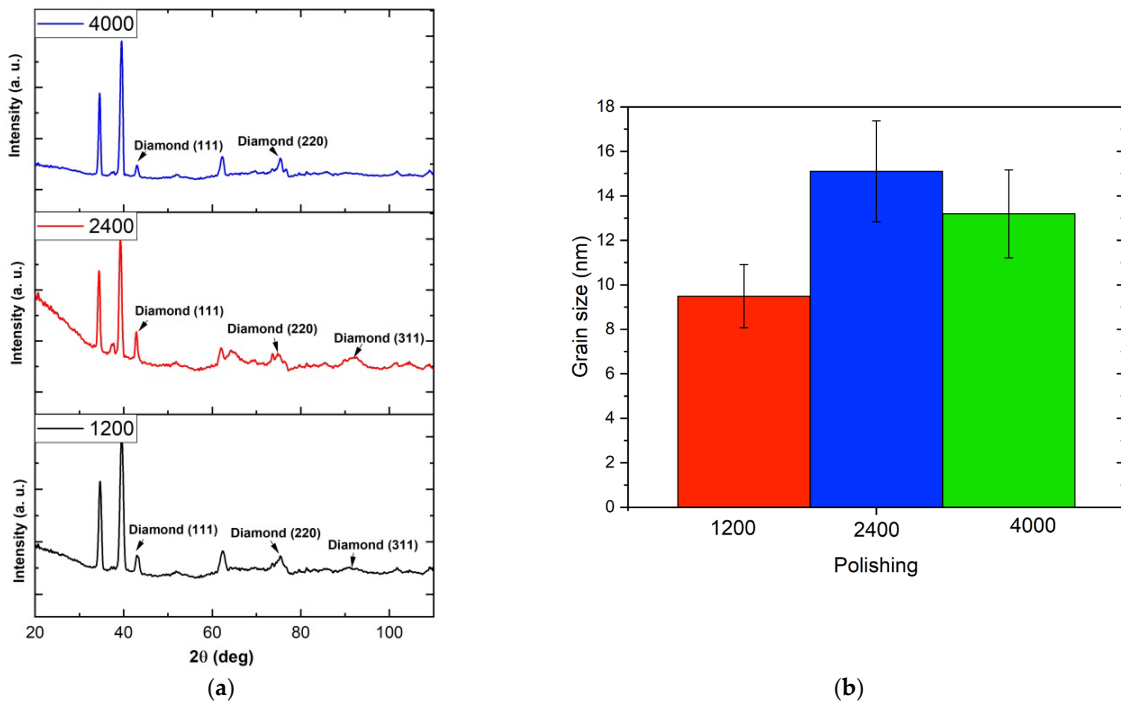


**Figure 4.** (a) X-ray diffraction patterns of diamond thin films grown on TA6V substrates polished with the three different polishing grades and (b) estimated grain size.

A first-hand estimation of the surface roughness after polishing and after NCD deposition was obtained by profilometry measurements. Figure 5 reports the values of the arithmetic average roughness (Ra) thus estimated. The roughness of the TA6V substrates decreases from 90 to 50 nm when the polishing granulometry decreases from 1200 to 4000. The same behavior is observed after diamond deposition, but with higher values that decay from 150 to 110 nm. Therefore, the NCD deposition provokes a significant increase in the surface topography, whereas, as expected, the use of a smaller granulometry for polishing leads to a smoother substrate surface.

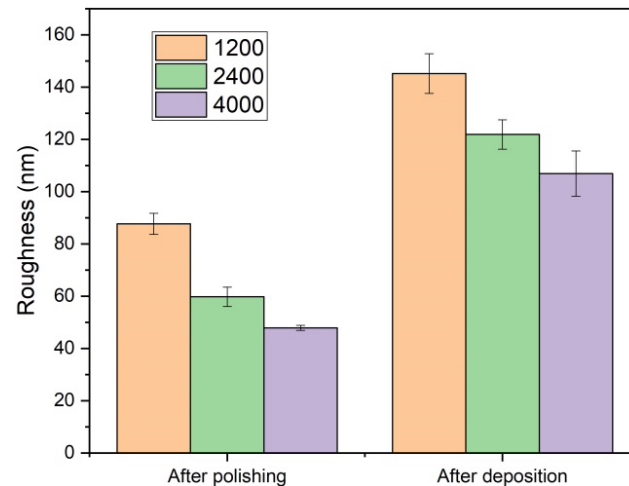


**Figure 5.** Roughness Ra measured by profilometry for the six configurations considered in the study: TA6V and NCD/TA6V obtained by polishing samples with granulometry 1200, 2400, and 4000.

Thorough measurements of the 3D roughness were achieved on an interferometer using a 50 $\times$  objective (Zygo). The vertical resolution of the machine in this configuration is lower than 10 nm, typically 8 to 9 nm, and the lateral resolution is equal to 0.52  $\mu\text{m}$  (Figure 6).

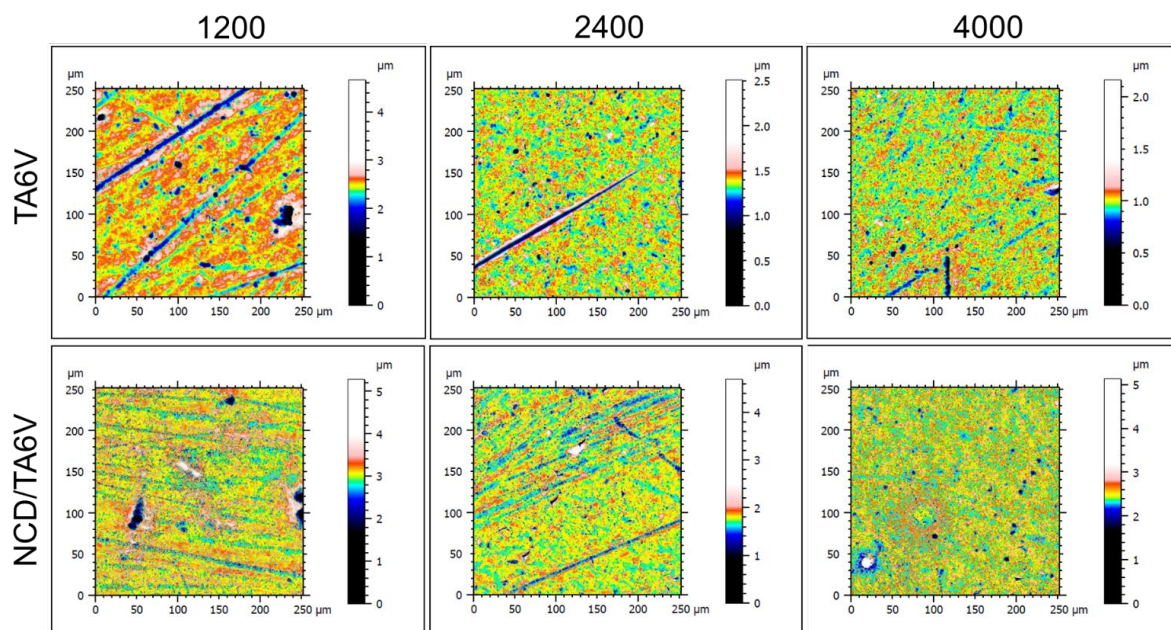


**Figure 6.** The 3D experimental measurements of the six configurations considered in the study: TA6V and NCD/TA6V obtained by polishing samples with granulometry 1200, 2400, and 4000.

After computation and analysis of the 43 roughness parameters, four parameters came to our attention:

- $S_{tr}$ : Spatial parameter (ISO 25178): Texture-aspect ratio;
- $S_a$  ( $\mu\text{m}$ ): Amplitude parameter (ISO 25178): Arithmetic mean height;
- $S_{ku}$ : Amplitude parameter (ISO 25178): Kurtosis;
- $V_{vv}$  ( $\text{mm}^3/\text{mm}^2$ ): Volume functional parameters: Pit void volume.

The results are summarized in Table 1.

**Table 1.** Average and standard deviation of the considered roughness parameters.

Sample	$S_{tr}$		$S_a$ ( $\mu\text{m}$ )		$S_{ku}$		$V_{vv}$ ( $\text{mm}^3/\text{mm}^2$ )	
	Average	Standard Deviation	Average	Standard Deviation	Average	Standard Deviation	Average	Standard Deviation
TA6V <sub>1200</sub>	0.42	0.18	0.12	0.03	18.38	26.93	0.03	0.01
NCD/TA6V <sub>1200</sub>	0.52	0.24	0.2	0.06	6.36	2.27	0.05	0.02
TA6V <sub>2400</sub>	0.6	0.31	0.08	0.01	20.72	25.5	0.02	0.01
NCD/TA6V <sub>2400</sub>	0.82	0.09	0.18	0.05	7.7	4.34	0.05	0.01
TA6V <sub>4000</sub>	0.82	0.1	0.07	0.01	21.59	19.66	0.02	0.01
NCD/TA6V <sub>4000</sub>	0.76	0.23	0.19	0.06	6.36	2.27	0.04	0.02

The  $S_{tr}$  parameter is a measurement of the uniformity of the surface texture. This parameter shows an increase between TA6V1200 vs. 2400 vs. 4000, referring to a reduction in the textured appearance as a function of polishing grit, which was expected. This result can be explained by the disappearance or attenuation of polishing scratches caused by larger-grit sandpapers. The second result of the analysis of this parameter ( $S_{tr}$ ) shows that the presence of diamond coatings reduces the texturing effect (TA6V1200 vs. NCD/TA6V1200, respectively, TA6V2400 vs. NCD/TA6V2400), except for TA6V4000 and NCD/TA6V4000, where the results are similar. However, the values remain higher than 0.5, which reflects a good surface homogeneity in all directions [28].

When comparing the results without diamond (TA6V1200 vs. 2400 vs. 4000), it is interesting to note that the  $S_a$  parameter decreases, which seems logical and is consistent with the profilometry observations. The presence of diamond causes an increase by a factor 2 in this parameter and gives a similar value regardless of the polishing protocol, which differs significantly from the  $R_a$  variation reported using profilometry. According to interferometry measurements, the addition of diamond therefore increases the surface roughness locally while stabilizing this level of roughness regardless of the polishing protocol used. A comparative behavior has been observed by Mordo et al. [29] when investigating the deposition of DLC films. Indeed, whatever the initial roughness of the bare substrates, the coating with DLC films thick enough leads to surface roughness roughly identical after DLC deposition. This is an interesting result to consider in order to overcome polishing defects and to reduce variability between samples.

The  $S_{ku}$  value is a measure of the sharpness of the roughness profile. If  $S_{ku} < 3$ , the height distribution is asymmetrical above the mean plane, whereas if  $S_{ku} > 3$ , the height distribution is peaked. The distribution in this study is then in peak form for each sample. This parameter is similar for the three samples without diamond, with values between 18.38 and 21.59. Such elevated values ( $S_{ku} > 5$ ) reveal the existence of irregular and repetitive local structures [30]. With values between 6.36 and 7.7 for the three coated samples, the addition of diamond films reduces the value of this parameter, so the elementary surface becomes smaller and approaches a surface that can be described as a sand-blasted surface with the presence of peaks and valleys. These new peaks are wider and smoother, comparable to sinusoids. This can be associated with the shape of the grains that form the DNC films, since it is expected that the near spherical shape of the diamond particles negatively affects the kurtosis values [31]. Nevertheless, these values remain above 3, which is very promising, because it has been demonstrated that for titanium implant surfaces, kurtosis values higher

than 3 have a positive effect on the implant preservation related to bone and ensure a good cell adhesion [32].

The  $V_{vv}$  value represents the void volume of the valleys for the value  $p\%$  of the surface material ratio. The results of this parameter are similar for the three samples without diamond, between 0.2 and 0.3, and for the three samples with diamond, between 0.4 and 0.5. The addition of diamonds thus increases the value of this parameter; the surface becomes more hilly. However, the observed valleys are smaller, which is in good agreement with the previous roughness parameter  $S_{ku}$ .

The hardness of the considered samples was investigated using a microdurometer. Table 2 summarizes the results (average and standard deviation of Vickers hardness, Anova and Tukey Kramer tests) obtained for the six configurations considered in the study, i.e., TA6V substrates polished with granulometry 1200, 2400, and 4000 with and without NCD coatings. Comparable results in terms of order of magnitude are obtained for polishing samples with 1200 and 2400 (TA6V<sub>1200</sub> vs. TA6V<sub>2400</sub> and NCD/TA6V<sub>1200</sub> vs. NCD/TA6V<sub>2400</sub>). In particular, an increase in Vickers hardness is obtained for the samples polished with the 4000 abrasive paper (cf. TA6V<sub>4000</sub> and NCD/TA6V<sub>4000</sub>).

**Table 2.** Average and standard deviation of microhardness for the six configurations considered in the study: TA6V and NCD/TA6V obtained by polishing samples with granulometry 1200, 2400, and 4000. Anova and Tukey Kramer tests show the significant effects of diamond deposits, with two statistically significant differences referenced as \* and \*\*.

Sample	Hardness (HV)		Statistical Tests	
	Average	Standard Deviation	ANOVA	Tukey Kramer
TA6V <sub>1200</sub>	320.24	4.00	$p = 0.0267$	*
NCD/TA6V <sub>1200</sub>	329.92	12.91		*
TA6V <sub>2400</sub>	321.58	10.63		
NCD/TA6V <sub>2400</sub>	328.3	5.71		
TA6V <sub>4000</sub>	334.18	5.25		
NCD/TA6V <sub>4000</sub>	341.28	15.63		**

ANOVA shows a significant effect of diamond coatings ( $p < 0.05$ ). The Tukey Kramer test shows a statically significant difference between NCD/TA6V<sub>4000</sub> (referenced as \*\* in Table 2) and the samples polished with the 1200 and 2400 abrasive paper (TA6V<sub>1200</sub> and NCD/TA6V<sub>2400</sub>) (referenced as \* in Table 2). The results shown in Table 2 are compiled in Figure 7.

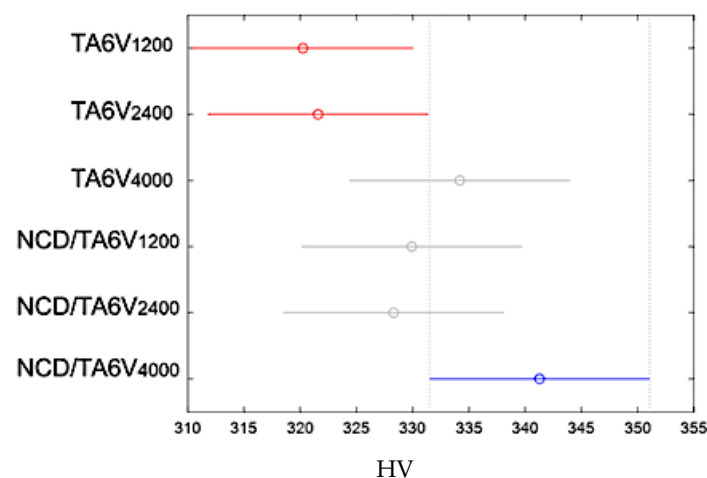


**Figure 7.** Results of Tukey Kramer test: two groups (TA6V<sub>1200</sub> and TA6V<sub>2400</sub>) have means significantly different from NCD/TA6V<sub>4000</sub>.

The increase in hardness when comparing the groups with and without diamond is an expected result. Indeed, the addition of a diamond film increases the properties of the test material [33,34]. It is important to note that a similarity is observed in the TA6V1200 and TA6V2400 results (NCD/TA6V1200 and NCD/TA6V2400, respectively) and an increase in the hardness value for TA6V4000 (NCD/TA6V4000). This effect may be related to the work-hardening phenomenon arising from the polishing process. The surface treatment increases the surface roughness by the impingement. The use of small abrasive particles results in localized plastic strain. Furthermore, this impingement produces an increase in the surface hardness due to the compressive load of the impact of the particles. Such hardening occurs most notably for ductile materials such as the titanium alloy [35,36].

#### 4. Conclusions

In this paper, the TA6V roughness effects on the characteristics of nanocrystalline diamond films deposited using a distributed antenna array microwave reactor were investigated.

NCD coatings were thus successfully achieved on the considered TA6V samples polished with 15  $\mu\text{m}$ , 9  $\mu\text{m}$ , and 5  $\mu\text{m}$  grain size, referenced as 1200, 2400, and 4000 polishing grit, respectively. Their morphology, purity, and microstructure are comparable to those obtained on substrates such as silicon wafer in the same reactor and growth conditions.

The polishing degree has no significant effect on diamond nucleation and growth but plays an important role on the roughness parameters and hardness of the NCD thin films.

The deposition of diamond leads to characteristic surface changes in appearance and size:

- The transformation of the peaks into sinusoids ( $S_{ku}$ ) leads to a homogenization of the surface (stochastic surface) ( $S_{tr}$ );
- The presence of these sinusoids forms valleys ( $V_{vv}$ ) of smaller characteristic size and reinforces the homogenization of the surface ( $S_{tr}$ );
- All this leads to an increase in the average roughness ( $S_a$ ) and a harmonization of the surface regardless of the polishing protocol used (1200 vs. 2400 vs. 4000 abrasive paper).

The enhanced hardness value for 4000 polishing grit can probably be attributed to the work-hardening phenomenon. The significant increase in the TA6V hardness due to NCD coating is thus very promising for the improvement of the resistance to wear of TA6V implants, which may increase the medical devices' durability.

Forthcoming works will deal with the biological evaluation (cytotoxicity, cell viability, osteointegration) of TA6V disks polished with different polishing grit and coated with NCD layers, aimed at linking the surface roughness and the sample hardness with biomedical predispositions of NCD/TA6V systems.

**Author Contributions:** Formal analysis, A.V.O., C.M. and R.V.; investigation, A.V.O., C.M. and R.V.; data curation, C.M.; writing—original draft preparation, A.V.O. and R.V.; writing—review and editing, F.B.; supervision, C.F.-D. and F.B.; project administration, C.F.-D. and F.B. All authors have read and agreed to the published version of the manuscript.

**Funding:** ANR (Agence Nationale de la Recherche) and CGI (Commissariat à l'Investissement d'Avenir) are gratefully acknowledged for their financial support of this work through Labex SEAM (Science and Engineering for Advanced Materials and devices), ANR-10-LABX-096 and ANR-18-IDEX-0001.

**Institutional Review Board Statement:** Not applicable.

**Informed Consent Statement:** Not applicable.

**Data Availability Statement:** Not applicable.

**Conflicts of Interest:** The authors declare no conflict of interest.

## References

1. Black, J. *Biological Performance of Materials: Fundamentals of Biocompatibility*, 4th ed.; CRC Press: Boca Raton, FL, USA, 2006.
2. Lampin, M.; Warocquier-Clérout, R.; Legris, C.; Degrange, M.; Sigot-Luizard, M.F. Correlation between substratum roughness and wettability, cell adhesion, and cell migration. *J. Biomed. Mater. Res. Off. J. Soc. Biomater. Jpn. Soc. Biomater.* **1997**, *36*, 99–108. [[CrossRef](#)]
3. MacDonald, D.; Deo, N.; Markovic, B.; Stranick, M.; Somasundaran, P. Adsorption and dissolution behavior of human plasma fibronectin on thermally and chemically modified titanium dioxide particles. *Biomaterials* **2001**, *23*, 1269–1279. [[CrossRef](#)] [[PubMed](#)]
4. Sandrini, E.; Morris, C.; Chiesa, R.; Cigada, A.; Santin, M. In vitro assessment of the osteointegrative potential of a novel multiphase anodic spark deposition coating for orthopaedic and dental implants. *J. Biomed. Mater. Res. Part B Appl. Biomater.* **2005**, *73B*, 392–399. [[CrossRef](#)] [[PubMed](#)]
5. Neel, E.A.A.; Mizoguchi, T.; Ito, M.; Bitar, M.; Salih, V.; Knowles, J.C. In vitro bioactivity and gene expression by cells cultured on titanium dioxide doped phosphate-based glasses. *Biomaterials* **2007**, *28*, 2967–2977. [[CrossRef](#)]
6. Skoog, S.A.; Kumar, G.; Zheng, J.; Sumant, A.V.; Goering, P.L.; Narayan, R.J. Biological evaluation of ultrananocrystalline and nanocrystalline diamond coatings. *J. Mater. Sci. Mater. Med.* **2016**, *27*, 1–13. [[CrossRef](#)]
7. Dekkar, D.; Bénédict, F.; Falentin-Daudré, C.; Rangel, A.; Issaoui, R.; Migonney, V.; Achard, J. Microstructure and biological evaluation of nanocrystalline diamond films deposited on titanium substrates using distributed antenna array microwave system. *Diam. Relat. Mater.* **2020**, *103*, 107700. [[CrossRef](#)]
8. Al-Azizi, A.A.; Eryilmaz, O.; Erdemir, A.; Kim, S.H. Nano-texture for a wear-resistant and near-frictionless diamond-like carbon. *Carbon* **2014**, *73*, 403–412. [[CrossRef](#)]
9. Bernal, R.A.; Chen, P.; Schall, J.D.; Harrison, J.A.; Jeng, Y.-R.; Carpick, R.W. Influence of chemical bonding on the variability of diamond-like carbon nanoscale adhesion. *Carbon* **2018**, *128*, 267–276. [[CrossRef](#)]
10. Țălu, Ș.; Bramowicz, M.; Kulesza, S.; Ghaderi, A.; Dalouji, V.; Solaymani, S.; Kenari, M.F.; Ghoranneviss, M. Fractal features and surface micromorphology of diamond nanocrystals. *J. Microsc.* **2016**, *264*, 143–152. [[CrossRef](#)]
11. Schade, A.; Rosiwal, S.M.; Singer, R.F. Influence of surface topography of HF-CVD diamond films on self-mated planar sliding contacts in dry environments. *Surf. Coatings Technol.* **2007**, *201*, 6197–6205. [[CrossRef](#)]
12. Kovalchenko, A.; Elam, J.; Erdemir, A.; Carlisle, J.; Auciello, O.; Libera, J.; Pellin, M.; Gruen, D.; Hryn, J. Development of ultrananocrystalline diamond (UNCD) coatings for multipurpose mechanical pump seals. *Wear* **2011**, *270*, 325–331. [[CrossRef](#)]
13. Jacobs, T.D.B.; Ryan, K.E.; Keating, P.L.; Grierson, D.S.; Lefever, J.A.; Turner, K.T.; Harrison, J.A.; Carpick, R.W. The Effect of Atomic-Scale Roughness on the Adhesion of Nanoscale Asperities: A Combined Simulation and Experimental Investigation. *Tribol. Lett.* **2013**, *50*, 81–93. [[CrossRef](#)]
14. Ryan, K.E.; Keating, P.L.; Jacobs, T.D.B.; Grierson, D.S.; Turner, K.T.; Carpick, R.W.; Harrison, J.A. Simulated Adhesion between Realistic Hydrocarbon Materials: Effects of Composition, Roughness, and Contact Point. *Langmuir* **2014**, *30*, 2028–2037. [[CrossRef](#)]
15. Alcaide, M.; Papaioannou, S.; Taylor, A.; Fekete, L.; Gurevich, L.; Zachar, V.; Pennisi, C.P. Resistance to protein adsorption and adhesion of fibroblasts on nanocrystalline diamond films: The role of topography and boron doping. *J. Mater. Sci. Mater. Med.* **2016**, *27*, 1–12. [[CrossRef](#)] [[PubMed](#)]
16. Mehedi, H.-A.; Achard, J.; Rats, D.; Brinza, O.; Tallaire, A.; Mille, V.; Silva, F.; Provent, C.; Gicquel, A. Low temperature and large area deposition of nanocrystalline diamond films with distributed antenna array microwave-plasma reactor. *Diam. Relat. Mater.* **2014**, *47*, 58–65. [[CrossRef](#)]
17. Nave, A.; Baudrillart, B.; Hamann, S.; Bénédict, F.; Lombardi, G.; Gicquel, A.; Van Helden, J.H.; Ropcke, J. Spectroscopic study of low pressure, low temperature H<sub>2</sub>–CH<sub>4</sub>–CO<sub>2</sub> microwave plasmas used for large area deposition of nanocrystalline diamond films. Part I: On temperature determination and energetic aspects. *Plasma Sources Sci. Technol.* **2016**, *25*, 065002. [[CrossRef](#)]
18. Nave, A.; Baudrillart, B.; Hamann, S.; Bénédict, F.; Lombardi, G.; Gicquel, A.; Van Helden, J.H.; Ropcke, J. Spectroscopic study of low pressure, low temperature H<sub>2</sub>–CH<sub>4</sub>–CO<sub>2</sub> microwave plasmas used for large area deposition of nanocrystalline diamond films. Part II: On plasma chemical processes. *Plasma Sources Sci. Technol.* **2016**, *25*, 065003. [[CrossRef](#)]
19. Baudrillart, B.; Bénédict, F.; Brinza, O.; Bieber, T.; Chauveau, T.; Achard, J.; Gicquel, A. Microstructure and growth kinetics of nanocrystalline diamond films deposited in large area/low temperature distributed antenna array microwave-plasma reactor. *Phys. Status Solidi A* **2015**, *212*, 2611–2615. [[CrossRef](#)]
20. Monshi, A.; Foroughi, M.R.; Monshi, M.R. Modified Scherrer Equation to Estimate More Accurately Nano-Crystallite Size Using XRD. *World J. Nano Sci. Eng.* **2012**, *02*, 154–160. [[CrossRef](#)]
21. Rietveld, H.M. Line profiles of neutron powder-diffraction peaks for structure refinement. *Acta Crystallogr.* **1967**, *22*, 151–152. [[CrossRef](#)]
22. Deltombe, R.; Kubiak, K.J.; Bigerelle, M. How to select the most relevant 3D roughness parameters of a surface. *Scanning* **2013**, *36*, 150–160. [[CrossRef](#)] [[PubMed](#)]
23. Baudrillart, B.; Bénédict, F.; Chauveau, T.; Bartholomot, A.; Achard, J. Nanocrystalline diamond films grown at very low substrate temperature using a distributed antenna array microwave process: Towards polymeric substrate coating. *Diam. Relat. Mater.* **2017**, *75*, 44–51. [[CrossRef](#)]
24. Ferrari, A.C.; Robertson, J. Raman spectroscopy of amorphous, nanostructured, diamond-like carbon, and nanodiamond. *Philos. Trans. R. Soc. A Math. Phys. Eng. Sci.* **2004**, *362*, 2477–2512. [[CrossRef](#)]

25. Hu, L.; Guo, Y.; Du, S.; Tian, S.; Li, J.; Gu, C. Probing trans-polyacetylene segments in a diamond film by tip-enhanced Raman spectroscopy. *Diam. Relat. Mater.* **2021**, *116*, 108415. [[CrossRef](#)]
26. Mahi, C.; Brinza, O.; Issaoui, R.; Achard, J.; Bénédic, F. Synthesis of High Quality Transparent Nanocrystalline Diamond Films on Glass Substrates Using a Distributed Antenna Array Microwave System. *Coatings* **2022**, *12*, 1375. [[CrossRef](#)]
27. Al-Rubaie, K.S.; Melotti, S.; Rabelo, A.; Paiva, J.M.; Elbestawi, M.A.; Veldhuis, S.C. Machinability of SLM-produced Ti6Al4V titanium alloy parts. *J. Manuf. Process.* **2020**, *57*, 768–786. [[CrossRef](#)]
28. Gambardella, A.; Marchiori, G.; Maglio, M.; Russo, A.; Rossi, C.; Visani, A.; Fini, M. Determination of the Spatial Anisotropy of the Surface MicroStructures of Different Implant Materials: An Atomic Force Microscopy Study. *Materials* **2021**, *14*, 4803. [[CrossRef](#)] [[PubMed](#)]
29. Mordo, S.; Popravko, V.; Barari, A. Study of the Effect of Coating Parameters and Substrates on 3D Surface Roughness in Diamond-Like-Carbon Coating Process. *IFAC Proc. Vol.* **2013**, *46*, 1861–1866. [[CrossRef](#)]
30. Zhang, H.-S.; Endrino, J.; Anders, A. Comparative surface and nano-tribological characteristics of nanocomposite diamond-like carbon thin films doped by silver. *Appl. Surf. Sci.* **2008**, *255*, 2551–2556. [[CrossRef](#)]
31. Lerebours, A.; Vigneron, P.; Bouvier, S.; Rassineux, A.; Bigerelle, M.; Egles, C. Additive manufacturing process creates local surface roughness modifications leading to variation in cell adhesion on multifaceted TiAl6V4 samples. *Bioprinting* **2019**, *16*, e00054. [[CrossRef](#)]
32. Lamolle, S.F.; Monjo, M.; Lyngstadaas, S.P.; Ellingsen, J.E.; Haugen, H.J. Titanium implant surface modification by cathodic reduction in hydrofluoric acid: Surface characterization and in vivo performance. *J. Biomed. Mater. Res. Part A* **2008**, *88A*, 581–588. [[CrossRef](#)] [[PubMed](#)]
33. Catledge, S.A.; Borham, J.; Vohra, Y.K.; Lacefield, W.R.; Lemons, J.E. Nanoindentation hardness and adhesion investigations of vapor deposited nanostructured diamond films. *J. Appl. Phys.* **2002**, *91*, 5347–5352. [[CrossRef](#)]
34. Pareta, R.; Yang, L.; Kothari, A.; Sirinrath, S.; Xiao, X.; Sheldon, B.W.; Webster, T.J. Tailoring nanocrystalline diamond coated on titanium for osteoblast adhesion. *J. Biomed. Mater. Res. Part A* **2010**, *95A*, 129–136. [[CrossRef](#)] [[PubMed](#)]
35. Xia, Y.; Bigerelle, M.; Marteau, J.; Mazeran, P.-E.; Bouvier, S.; Iost, A. Effect of surface roughness in the determination of the mechanical properties of material using nanoindentation test. *Scanning* **2013**, *36*, 134–149. [[CrossRef](#)] [[PubMed](#)]
36. Aparicio, C.; Rodriguez, D.; Gil, F.J. The effect of shot blasting and heat treatment on the fatigue behavior of titanium for dental implant applications. *Dent. Mater.* **2007**, *23*, 486–491. [[CrossRef](#)]

**Disclaimer/Publisher’s Note:** The statements, opinions and data contained in all publications are solely those of the individual author(s) and contributor(s) and not of MDPI and/or the editor(s). MDPI and/or the editor(s) disclaim responsibility for any injury to people or property resulting from any ideas, methods, instructions or products referred to in the content.